Optimized eight-dimensional lattice modulation format for IM-DD 56 Gb/s optical interconnections using 850 nm VCSELs

Lu, Xiaofeng; Tatarczak, Anna; Lyubopytov, Vladimir; Tafur Monroy, Idelfonso

Published in:
Journal of Lightwave Technology

Link to article, DOI:
10.1109/JLT.2017.2656389

Publication date:
2017

Document Version
Peer reviewed version

Optimized Eight-Dimensional Lattice Modulation Format for IM-DD 56 Gbit/s Optical Interconnections Using 850 nm VCSELs

Xiaofeng Lu, *Member, IEEE,* Anna Tatarczak, *Member, IEEE,*
Vladimir Lyubopytov, *Member, IEEE,* and Idelfonso Tafur Monroy, *Senior Member, IEEE*

(Invited Paper)

***Abstract*—In this paper a novel eight-dimensional lattice optimized modulation format, Block Based 8-dimensional/8-level (BB8), is proposed, taking into account the trade-off between high performance and modulation simplicity. We provide an experimental performance comparison with its n-level pulse amplitude modulation (PAM-n) counterparts in a 28 GBaud 850 nm vertical-cavity surface-emitting laser (VCSEL) based intensity-modulation direct-detection (IM-DD) system. Successful data transmission over 100 m multi-mode fiber (MMF) links of OM3 and OM4 types is demonstrated, with a power margin close to 2 dB at 100GBASE-SR4 forward error correction (FEC) threshold. A simplified bit-to-symbol mapping and corresponding symbol-to-bit de-mapping algorithms, together with a hyper-space hard-decision, are designed specifically for applications of short-reach data links. These algorithms are expected to use affordable computational resources with relatively low latency.**

***Index Terms*—Optical fiber communication, optical interconnections, modulation, vertical cavity surface emitting lasers.**

I. Introduction

DATA centers are increasingly becoming the infrastructure in the data era. The tremendous volume of the data flood merged and exchanged within and between data centers poses ever more demanding requirements on data links in terms of capacity, reach, cost, footprint, latency and power consumption. Intensity-modulation direct-direction (IM-DD) schemes are a good trade-off between the above-mentioned factors. Therefore, the majority of current generation short-reach optical interconnects are IM-DD based. Data links using multi-mode vertical-cavity surface-emitting lasers (MM-VCSELs) at 850 nm and multi-mode fibers (MMFs) are commonly used inside the data centers. They are relatively cheap due to easier system alignment and offer smooth upgrades by reusing the available facilities. In terms of capacity, the recent record is a 71 Gbps NRZ transmission in VCSEL-based link over 7 m MMF [1], with two-taps FFE and a 43 Gbps non-equalized transmission over 100 m OM3 MMF.

Advanced modulation formats are used to further enhance the link capacity. A promising format is the n-level pulse amplitude modulation (PAM-n) due to its higher spectral efficiency and easier implementation than that of other proposed modulation formats. An equalized PAM-4 is reported at 70 Gbps in a 2 m MMF link [2] and at 48.7 Gbps in 200 m OM4 MMF link [3]. Moreover, un-equalized PAM-8 is presented at 37.5 Gbps over 100 m OM4 [4]. The alternatives that allow for higher capacity at the cost of increased transceiver complexity are discrete multi-tone (DMT) [5] and multi-band carrierless amplitude phase modulation (Multi-CAP) [6]. Instead, in this paper we emphasize better system BER performance by using a multi-dimensional modulation format.

Multi-dimensional modulation (MD) formats have already been theoretically and experimentally investigated in coherent detection systems, e.g. the four-dimensional formats [7]–[14]. Besides, formats optimized with D_4 lattice can be equivalently obtained from the conventional PDM-mQAM by applying a four-dimensional set partitioning scheme [15]. Eight-dimensional formats have also been investigated recently [16]–[18]. A higher dimensional one, binary 24-dimensional modulation format, is also discussed in [19].

The pioneer theoretical works on the MD modulation formats for IM-DD systems include the optimized constellations for single-subcarrier IM transmission [20] and lattice code [21]. Recently, MD coded modulation has been experimentally validated in IM-DD systems. A two-dimensional coded modulation scheme with external modulators is discussed in [22]. A four-dimensional version is reported in [23]. A four-dimensional trellis coded modulation (TCM) is experimentally analyzed in [24] and [25]. A six-level four-dimensional format is numerically investigated in [26]. Yet, higher dimensional formats for VCSEL-based IM-DD transmission systems are not reported yet.

In this work, we theoretically propose and experimentally validate an alternative *block-based 8-dimensional/8-level* format, namely BB8, which carries 2 bits per symbol, i.e. has the same spectral efficiency as PAM-4. This paper is based on our recent conference paper reported in [27]. The fundamentals of eight-dimensional formats, including the optimization principles and geometric structure of BB8, are explained in Section II. In Section III the design of simplified algorithms for bit-to-symbol mapping and corresponding de-mapping is addressed as a trade-off between the performance and the modulation simplicity. The details of the corresponding hyper-space based hard-decision algorithm are given in Section IV. BB8 was ex-

X. Lu, A. Tatarczak, V. Lyubopytov and I. T. Monroy are with the Department of Photonics Engineering, Technical Unversity of Denmark, DK-2800, Kgs. Lyngby, Denmark. I. T. Monroy is also with ITMO University, St. Petersburg, Russia. e-mail: xilu@fotonik.dtu.dk; atat@fotonik.dtu.dk; vladly@fotonik.dtu.dk; idtm@fotonik.dtu.dk.

Manuscript received XXX XX, 2016; revised XXX XX, 2016.

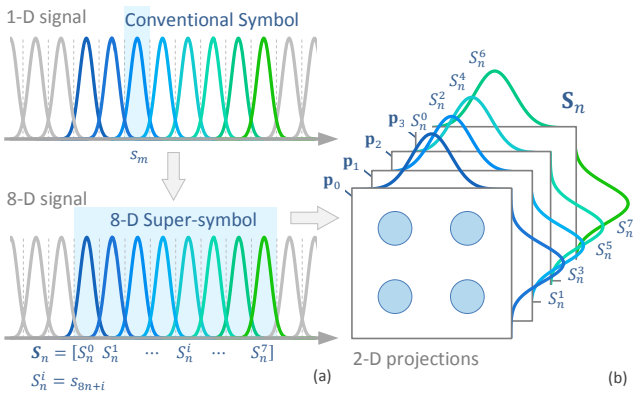

Fig. 1. (a) Illustration of the principle of constructing the eight-dimensional super-symbols by combining the temporally adjacent symbols. (b) The construction of two-dimensional projections by using two symbols.

perimentally investigated and compared with PAM-n in terms of BER in a 28 GBd lab setup. The performance was measured for back-to-back (BTB) and over 100 m OM3 and OM4 type MMF links. The experimental setup and methodological issues are described in Section V, and the experiment results are presented in Section VI.

II. Eight-dimensional Modulation Formats

A. Multi-dimensional signal space

An n-element orthogonal basis spans an n-dimensional signal space, accommodating the modulation formats of corresponding dimension. For instance, in coherent transmission systems the in-phase (I) and quadrature (Q) field components in both orthogonal polarization states (x and y), i.e. $[I_x, Q_x, I_y, Q_y]$, span a four-dimensional signal space. The orthogonal basis can also be formed using different wavelengths, independent waveforms or spatial modes. Ideally, consecutive symbol slots can also be seen as independent basis, provided the inter-symbol interference (ISI) is negligible. Alternatively, an orthogonal basis can be found in parallel optical channels, like separate fibers for the 4-lane quad small form-factor pluggable (QSFP) or 8-lane octal small form-factor pluggable (OSFP) transceivers. Such channels are inherently multi-dimensional. Furthermore, higher dimensional space can be virtually formed by adopting a hybrid scheme. For instance, links using 4λ shortwave wavelength division multiplexing (SWDM) over 4-lane parallel channels are sixteen-dimensional. In this paper, an eight-dimensional signal space is constructed by combining eight adjacent symbols in a single channel. The resulting sequence of super-symbols is further interleaved into 8 blocks, emulating eight independent channels.

B. MD formats for IM-DD systems and optimization

Let us consider, without loss of generality, an 8-dimensional format, where eight temporally adjacent symbols in the transmitting sequence $\mathbf{s} = [s_0, s_1, ..., s_m, ...]^{\mathrm{T}}$ constitutes a super-symbol $\mathbf{S}_n = [S_n^0, S_n^1, S_n^2, ...S_n^i, ...S_n^7]^{\mathrm{T}}$. s_m indicates the m-th symbol in the transmitting sequence. S_n^i is the individual symbol in the n-th super-symbol. $i = 0, 1, ..., 7$ indicates its position in $\mathbf{S}_n$. $n = 0, 1, ...$ is the index of a super-symbol in the sequence. S_n^i corresponds to the symbol s_{8n+i} in $\mathbf{s}$, i.e. $m = 8n + i$. Therefore, each symbol in one super-symbol gives the coordinate value of one point in 8-dimensional signal space along a specific orthogonal direction. We assume that the received super-symbols $\mathbf{R}_n = [R_n^0, R_n^1, R_n^2...R_n^7]^{\mathrm{T}}$ are affected by additive white Gaussian noise (AWGN). They can be visualized as hyper-spheres expanded from the ideal format points, like $\mathbf{R}_n = \mathbf{S}_n + \mathbf{N}_n$, where $\mathbf{N}_n$ are independent and identically distributed (i.i.d.) random variables. Notice that here the channel responses are not taken into account, i.e. each super-symbol is seen as independent. In fact, the Gaussian model is not naturally guaranteed in VCSEL based IM-DD links, that leads to the noise spheres shifted from the designed locations and apart from the hyper-sphere form, becoming more irregular and anisotropic. The impact of this effect on the performance is not straightforward and depends on the specific constellation configuration. In this paper, we assume that the shift and distortion of the noise hyper-spheres are negligible and adopt a Gaussian noise model.

The modulation format can be optimized by maximizing the minimum mutual Euclidean distance (MMED), d_{min}, between all pairs of the format points to avoid the errors occurring in the overlap region between noise spheres. The optimal format is then achieved when the format points are chosen from the densest lattice. The densest eight-dimensional structure, called E_8 lattice, can be constructed in multiple ways [28]: (i) generation matrix; (ii) seed lattice grids; (iii) analytic expression, $E_8 = \left\{(x_i) \in \mathbb{Z}^8 \cup (\mathbb{Z} + 1/2)^8 : \sum_i x_i \equiv 0 \ (\mathrm{mod} 2)\right\}$. Assuming that the VCSEL is modulated in its linear regime, the optimization equals to searching a subset of E_8 lattice within a fixed-size eight-dimensional hypercube. Such subset has the maximum d_{min} and an optimal orientation, offering the simplest level structure in each symbol.

C. Block-based 8-dimensional/8-level format: BB8

BB8 has 8 equally probable amplitude levels. The format point set $\mathbf{C}$ is defined as:

$$\mathbf{C} = \left\{(c^i) \in \mathbf{U}_{even}^8 \cup \mathbf{U}_{odd}^8 : \sum_i c^i \equiv 0 \ (\mathrm{mod} 4)\right\} \quad (1)$$

where c^i is the amplitude of each symbol, $i = 0, 1, \cdots, 7$ is the position of individual symbol in a super-symbol, and $\mathbf{U}_{even}^{\lambda} = [u_{even}^0, u_{even}^1, ..., u_{even}^i, ..., u_{even}^{\lambda-1}]^{\mathrm{T}}$, $u_{even}^i \in \{0, 2, 4, 6\}$, $\mathbf{U}_{odd}^{\lambda} = [u_{odd}^0, u_{odd}^1, ..., u_{odd}^i, ..., u_{odd}^{\lambda-1}]^{\mathrm{T}}$, $u_{odd}^i \in \{1, 3, 5, 7\}$ are the sets of possible values, in which λ indicates the dimensionality of such sets. We can use the representation of two-dimensional projections to better understand the format structure in eight-dimensional space. As shown in Fig. 1, a super-symbol forms four two-dimensional projections by artificially projecting every two symbols in one constellation diagram. Without loss of generality, we define the projections as $\mathbf{p}_k = [\, c^{2k}\ c^{2k+1}\,]^{\mathrm{T}}, k = 0, 1, 2, 3$ with a symbol-wise sequence.

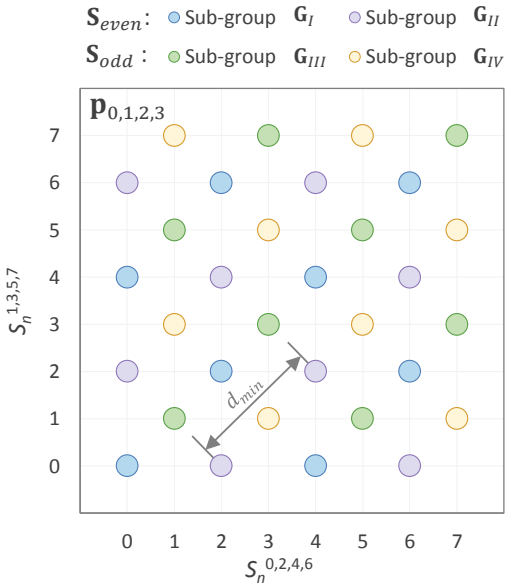

Fig. 2. Proposed formats illustrated with aids of 2D projection in constellation diagram. Illustration of the sub-groups $\mathbf{G}_I$ and $\mathbf{G}_{II}$ in the subset $\mathbf{S}_{even}$, $\mathbf{G}_{III}$ and $\mathbf{G}_{IV}$ in the subset $\mathbf{S}_{odd}$ on two-dimensional projection.

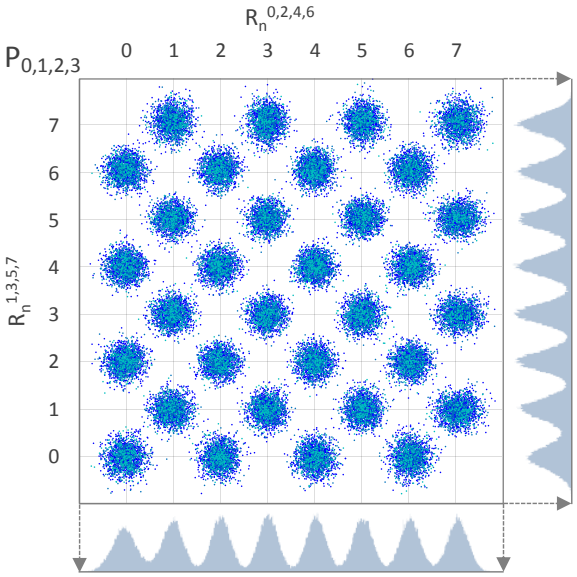

Fig. 3. Experimentally measured symbol histogram and its 2D projection.

According to the expression (1), the set of format $\mathbf{C}$ is divided into two independent subsets, i.e. even and odd subsets, with the expression $\mathbf{C}_{even} = \{(c^i) \in \mathbf{U}^8_{even} : \sum_i c^i \equiv 0(\text{mod}2)\}$ and $\mathbf{C}_{odd} = \{(c^i) \in \mathbf{U}^8_{odd} : \sum_i c^i \equiv 0(\text{mod}2)\}$. Format points in each projection $\mathbf{p}_k$ are then divided into four sub-groups (SG), as:
$\mathbf{G}_I = \{(c^i) \in \mathbf{U}^2_{even} : c^{2k} + c^{2k+1} \equiv 0(\text{mod}4), k = 0, 1, 2, 3\}$;
$\mathbf{G}_{II} = \{(c^i) \in \mathbf{U}^2_{even} : c^{2k} + c^{2k+1} \equiv 1(\text{mod}4), k = 0, 1, 2, 3\}$;
$\mathbf{G}_{III} = \{(c^i) \in \mathbf{U}^2_{odd} : c^{2k} + c^{2k+1} - 1 \equiv 0(\text{mod}4), k = 0, 1, 2, 3\}$;
$\mathbf{G}_{IV} = \{(c^i) \in \mathbf{U}^2_{odd} : c^{2k} + c^{2k+1} - 1 \equiv 1(\text{mod}4), k = 0, 1, 2, 3\}$.
They are represented by points of four different colors in Fig. 2. The even subset is constructed with a conditional combination of pairs in $\mathbf{G}_I$ and $\mathbf{G}_{II}$, meaning $\mathbf{C}_{even} = [\ \mathbf{p}_1\ \mathbf{p}_2\ \mathbf{p}_3\ \mathbf{p}_4\ ]^{\mathrm{T}}$, $\mathbf{p}_j \in \mathbf{G}_I \cup \mathbf{G}_{II}$, in which the number of pairs from $\mathbf{G}_I$ should be 0, 2 or 4, and 4, 2 or 0 from $\mathbf{G}_{II}$, correspondingly. The odd subset is constructed with a conditional combination in $\mathbf{G}_{III}$ and $\mathbf{G}_{IV}$, as: $\mathbf{C}_{odd} = [\ \mathbf{p}_1\ \mathbf{p}_2\ \mathbf{p}_3\ \mathbf{p}_4\ ]^{\mathrm{T}}$, $\mathbf{p}_k \in \mathbf{G}_{III} \cup \mathbf{G}_{IV}$ with similar condition as above mentioned.

BB8 carries 2 bits/symbol, the same as PAM-4. Therefore the format set $\mathbf{C}$ has $4^8 = 65536$ points. The MMED of neighboring points reaches $d_{min} = 2\sqrt{2}$. Theoretically, BB8 has a 0.84 dB asymptotic shaping gain compared to its PAM-n counterparts with the same maximum peak-to-peak modulation amplitude. Fig. 3 displays the aforementioned two-dimensional projection presented with experimental data, together with the histogram of the received symbols.

The proposed format is designed for independent parallel channels, where the orthogonality of the basis is inherently guaranteed. However, such assumption is not reasonable for the temporally adjacent symbols transmitted through 100 m MMF because the ISI resulting from the unavoidable inter-modal dispersion skews the basis. Hence we use a block-wise interleaving scheme to emulate the parallel channels. 64k symbols, i.e. 8k super-symbols, are fed into an interleaving matrix column-wisely. Then 8 blocks are generated row-wisely, with each block as an analogy of an independent channel. In other words, each output block contains the symbols having the same position in their original super-symbols. By doing so, the ISI becomes the signal independent noise. It is noteworthy that for keeping the consistency, we applied the same interleaving scheme on all the formats we investigate in this work.

A Monte Carlo simulation has been made based on AWGN model applied on the ideal constellations. Its results are shown in the Fig. 4. The signal-to-noise ratio is given with respect to the received electrical signal. PAM-4 and BB8 have an intersection point around the standard 7% FEC limit BER $\approx 3.8 \times 10^{-3}$. For low noise regime, BB8 outperforms PAM-4 and approaches the asymptotic gain larger than 0.8 dB.

III. Simplified Bit-to-Symbol Mapping and De-Mapping

In spite of the theoretical benefit, the practical implementation of MD formats is not straightforward due to the indirect bit-to-symbol mapping. Look-up tables (LUTs) can be a feasible solution for MD modulations with small scale constellations in coherent transmission systems. However, it cannot be applied for the highly latency- and cost-sensitive short-reach data links. A specially designed simplified bit-to-symbol algorithm is proposed in the following section. It is expected to enable the real-time bit-to-symbol mapping, and its corresponding de-mapping.

A. Bit-to-symbol mapping

For the input bit block $\mathbf{B}_n = [b_n^0\ b_n^1 \cdots b_n^e \cdots b_n^{15}]^{\mathrm{T}}$ and the mapped symbol sequence $\mathbf{S}_n = [S_n^0\ S_n^1 \cdots S_n^i \cdots S_n^7]^{\mathrm{T}}$, a bit-to-symbol mapping is defined as, $\mathcal{M} : \mathbf{F}_2^{16} \rightarrow \mathbb{R}^8$ and the corresponding symbol-to-bit de-mapping is $\mathcal{M}^{-1} : \mathbb{R}^8 \rightarrow \mathbf{F}_2^{16}$.

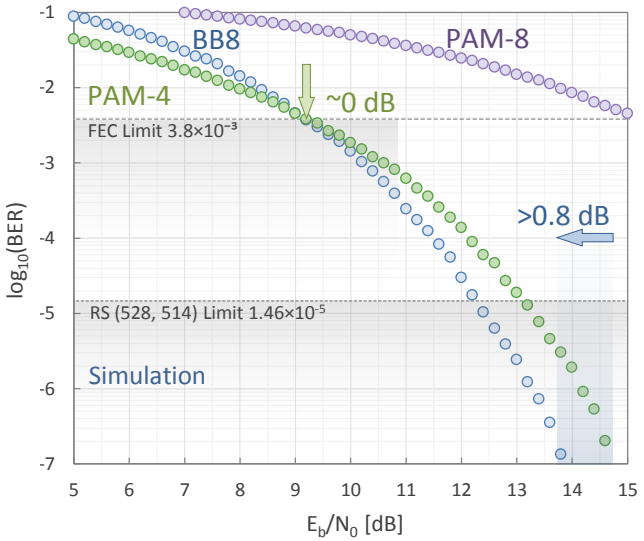

Fig. 4. Monte Carlo simulation of BB8, PAM-4 and PAM-8 with varying signal-to-noise ratio.

$\mathbf{F}_2^{16}$ means the 16-dimensional binary field. The superscript e indicates the position of the individual bit in $\mathbf{B}_n$. The simplified mapping algorithm is expressed as, $\mathcal{M}$:

$$S_n^0 = b_n^0 + 2b_n^1 + 4b_n^2 \quad (2)$$
$$S_n^1 = b_n^0 + 2b_n^3 + 4b_n^4 \quad (3)$$
$$S_n^2 = b_n^0 + 2b_n^5 + 4b_n^6 \quad (4)$$
$$S_n^3 = b_n^0 + 2b_n^7 + 4b_n^8 \quad (5)$$
$$S_n^4 = b_n^0 + 2b_n^9 + 4b_n^{10} \quad (6)$$
$$S_n^5 = b_n^0 + 2b_n^{11} + 4b_n^{12} \quad (7)$$
$$S_n^6 = b_n^0 + 2b_n^{13} + 4b_n^{14} \quad (8)$$
$$S_n^7 = b_n^0 + 2P_n + 4b_n^{15} \quad (9)$$

$$P_n = b_n^1 \oplus b_n^3 \oplus b_n^5 \oplus b_n^7 \oplus b_n^9 \oplus b_n^{11} \oplus b_n^{13} \quad (10)$$

In a mapping stage, every 16 bits are mapped into one 8-symbol super-symbol, with each symbol modulated into eight levels. The first bit (b_n^0) controls the selection of the candidate points from the even subsets (when $b_n^0 = 0$) or from odd ones (when $b_n^0 = 1$). Bits $b_n^1 ... b_n^{14}$ are simply mapped as PAM-4. It is noteworthy that they are not Gray mapped, since Gray mapping is not optimal in an eight-dimensional perspective. The last symbol is generated from bits b_n^0, b_n^{15} and a parity bit, P_n, which is calculated according to (10).

The merits of such bit-to-symbol mapping include: (i) minimizing the alteration from conventional PAM-4 mapping and therefore reducing the cost of IC design and implementation; (ii) minimizing extra computational resources required, as only additional calculation of parity bit P_n is needed; (iii) enabling real-time solution with lower latency relative to the other mapping schemes, e.g. LUT.

B. Symbol-to-bit de-mapping

The corresponding de-mapping algorithm is then written as:

$$b_n^0 = \mathrm{mod}(S_n^{0-7}, 2) \quad (11)$$
$$b_n^1 = \mathrm{mod}((S_n^0 - b_n^0)/2, 2) \quad (12)$$
$$b_n^2 = \mathrm{mod}((S_n^0 - b_n^0)/4, 2) \quad (13)$$
$$\cdots$$
$$b_n^{13} = \mathrm{mod}((S_n^6 - b_n^0)/2, 2) \quad (14)$$
$$b_n^{14} = \mathrm{mod}((S_n^6 - b_n^0)/4, 2) \quad (15)$$
$$b_n^{15} = \mathrm{mod}((S_n^7 - b_n^0)/2, 2) \quad (16)$$

In which, S_n^{0-7} means an arbitrary symbol from S_n^0 to S_n^7. During the de-mapping phase, a 16-bit block is recovered from one super-symbol, i.e. 8 received and aligned symbols. The first bit b_n^0 is decoded according to the parity of the subset that the received super-symbol belongs to, i.e. either even subset (when S_n^{0-7} is even, $b_n^0 = 0$) or odd subset (when S_n^{0-7} is odd, $b_n^0 = 1$). Then, the symbols S_n^{0-7} are shifted, i.e. subtracted by b_n^0, as described by Eq. 11-16. After doing that, S_n^{0-7} are degenerated from PAM-8 into PAM-4 signal. The remaining bits $b_n^1 ... b_n^{15}$ are simply calculated from S_n^{0-7} with PAM-4 de-mapper. The parity bit (P_n) is not used during the de-mapping and therefore discarded.

IV. Hyper-space Based Hard Decision

A maximum likelihood soft-decision (ML-SD) algorithm was used in coherent MD modulation systems. It is combined with FEC to maximize the achievable data rate [13]. However, considering the computational complexity, it is unrealistic to apply ML-SD to the eight-dimensional modulation. It would be overloaded by the number of possible states. In this work we propose a hyperspace based hard-decision (HS-HD) algorithm.

A lattice is filled with primitive cells, the smallest symmetric units. All positions inside the cell are closer to the center than to the rest of the lattice. Hence, the central lattice point in each primitive cell gives a decided symbol. All received symbols in one primitive cell have the same decision. We can separate an eight-dimensional primitive cell by determining all the perpendicular bisecting hyper-planes between the neighbors, as shown in Fig. 5. The perpendicular bisecting hyper-plane is also seen as the decision threshold hyper-plane. Generally, the (n-1)-dimensional boundaries of primitive cells work as hard-decision thresholds in an n-dimensional signal space. Hence, 7-dimensional hyper-planes $\mathbf{H}$ ($\mathbf{H} = \{\mathbf{x} \in \mathbb{R}^8 \mid \mathbf{a}^{\mathrm{T}}\mathbf{x} = d\}, \mathbf{a} = (a_1, a_1, \cdots, a_8)^{\mathrm{T}}$) divide the eight-dimensional signal space into cells of symbols. Here $\mathbf{x}$ represents the points on the hyper-plane and $\mathbf{a}$ is its normal vector.

We use a two-dimensional honeycomb (A_2 lattice) as the analog of the E_8 lattice to illustrate the principle of the algorithm (Fig. 5). Generally, the normal vector of the threshold plane between the j-th lattice point $\mathbf{l}_j \in \mathbf{L}$ and its z-th neighbor $\mathbf{l}_j^z \in \mathbf{L}$ is expressed as $\mathbf{a}^z = \mathbf{l}_j^z - \mathbf{l}_j$, where $\mathbf{L}$ is

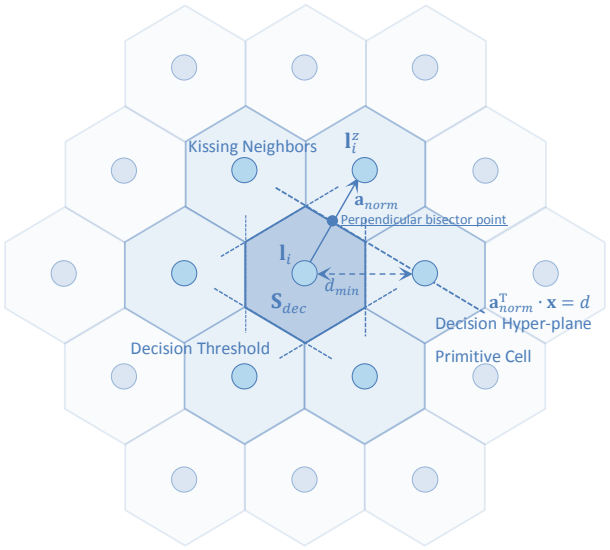

Fig. 5. Division of a signal space by using the decision threshold given by the perpendicular bisecting hyper-plane between a lattice point and its neighbors, apart from the origin of the coordinate by d_{min}, with the analogy of two-dimensional honeycomb structure (A_2 lattice).

the set of the whole lattice. The unit normal vector is then given as $\mathbf{a}_0^z = \mathbf{a}^z/d_{min}$. The perpendicular bisector of the line connecting these two points is described as $\mathbf{P} = \mathbf{l}_j + \mathbf{a}^z/2$. The hyper-plane function is written as $(\mathbf{a}_0^z)^{\mathrm{T}}\mathbf{x} = d$, in which $d = (\mathbf{a}_0^z)^{\mathrm{T}}\mathbf{P} = (\mathbf{a}_0^z)^{\mathrm{T}}(\mathbf{l}_j + \mathbf{a}^z/2) = D_j^z + d_{min}/2$. Here, d is the characteristic number, which equals the perpendicular distance between the decision plane and the origin of the coordinate; it consists of $d_{min}/2$, half of the MMED, and D_j^z, the perpendicular distance from the origin of the coordinate to the hyper-plane containing $\mathbf{l}_j$. $D_j^z \in \mathbf{D}^z$ is inherent for a specific lattice structure. $\mathbf{D}^z = (\mathbf{a}_0^z)^{\mathrm{T}}\mathbf{L}$ is the set of all possible D_j^z. Normally, due to the symmetry of the lattice, $\mathbf{D}^z$ degenerates to a smaller discrete set. It is evident that $\mathbf{D}^z$ consists of identical subsets equally spaced by distance d_{min} and expressed as $\mathbf{D}^z = \bigcup_{\mu=-\infty}^{\infty}(\mathbf{D}_0^z + \mu \cdot d_{min})$, $\mu \in \mathbb{Z}$. Specifically, the number of possible direction vectors $\mathbf{a}_0^z$ in E_8 reaches 120, because each E_8 lattice point is surrounded by 240 neighbors, and each direction has a conjugate counterpart, i.e. $\mathbf{a}_0^z = -\mathbf{a'}_0^z$, which reduces the number by half.

We use a 'cake-cutting' algorithm to implement the HS-HD. $d_n^z = (\mathbf{a}_0^z)^{\mathrm{T}}\mathbf{R}_n$ generates a characteristic number, which equals to the projection of $\mathbf{R}_n$ along the direction $\mathbf{a}_0^z$. The same procedure is applied on the lattice set $\mathbf{L}$ and generates a set of characteristic numbers, $\mathbf{D}^z$, as described above. By comparing the characteristic value d_n^z of the received super-symbol with the lattice characteristic values $D_\mu^z \in \mathbf{D}^z$, we obtain the difference $\delta = d_n^z - D_\mu^z$. Therefore, a hard decision selects a subset $\mathbf{L}^z$ of lattice from the whole set $\mathbf{L}$, where $|\delta| \leq d_{min}/2$. The selection starts from an arbitrary direction and goes through all possible 120 directions. The ergodic process stops when one element only remains in the candidate set. The procedure looks like cutting the cake (signal space) until the last piece containing the cherry (the decided symbol) is found.

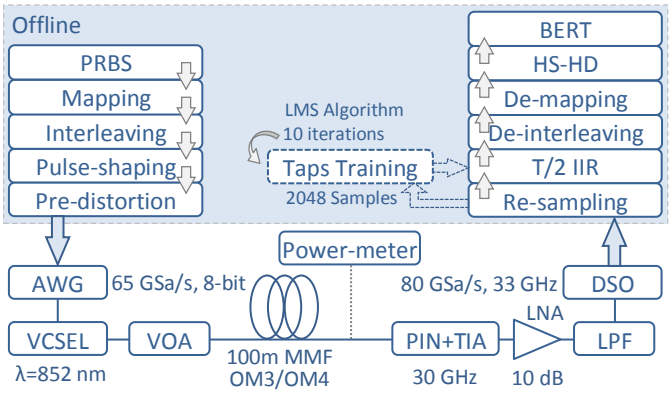

Fig. 6. Experimental setup used for BER measurements.

The major difference between HS-HD and the conventional hard-decision used for PAM-n are extra linear transforms required before the decision. Such operations are expected to be serialized with electrical analog circuits. As the decision can be implemented in an analog domain, ADC is dispensable, whereas it is required in the case of digital ML algorithms.

V. Experimental Validation

The experimental setup is presented in Fig. 6. A 850 nm multimode VCSEL, biased at 8 mA, is directly modulated by a 520 mV peak-to-peak differential electrical signal. A small-signal frequency response and an optical spectrum of the VCSEL are shown in Fig. 7 (a) and (b), respectively. The electrical signal is generated from 28 GBaud sequences of 256K symbols by a 65 GSa/s 8-bit arbitrary waveform generator (AWG). The sequences are pre-calculated with a raised cosine (roll-off factor 0.5) pulse shaping and repeatedly transmitted. A pre-equalization on the electrical signal is included to mitigate the spectral roll-off of the AWG. The VCSEL used in this experiment had a −3 dB bandwidth of 17 GHz. The maximum output optical power from the transmitter optical sub-assembly (TOSA) reaches −0.61 dBm. A variable optical attenuator (VOA) is employed, which has the insertion loss of 0.52 dB, reducing the maximum launched optical power to −1.13 dBm. The signal was received by a commercially available VI-Systems photo-diode package which includes a trans-impedance amplifier (TIA). The detected electrical signal was improved with a low-noise amplifier (LNA) and a low-pass filter (LPF). Signal traces were captured with a 33 GHz, 80 GSa/s digital storage oscilloscope (DSO). A back-to-back BER measurements were taken for a primary characterization. Then link measurements were performed with one spool of 100 m OM3 MMF and one of OM4 MMF. They introduce the losses of 0.69 dB and 0.85 dB respectively, giving the maximum received optical power −1.82 dBm and −1.98 dBm correspondingly. For convenience of comparison, we set −2 dBm as the maximum power for BER measurements in the following experiments and treat it as the maximum achievable received optical power.

The received digital signal was processed offline. The traces were resampled from 80 GSa/s to 56 GSa/s, i.e. two samples

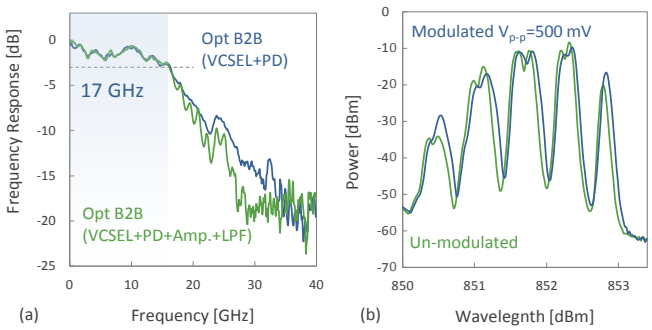

Fig. 7. (a) The end-to-end frequency response, with (lemon grass) and without (azure) post-amplifier and low pass filer. (b) The optical spectrum of VCSEL, with (azure) and without (lemon grass) electrical signal modulation.

per symbol, processed with a T/2 fractional infinite impulse response (IIR) filter with 11 and 5 taps in the feed-forward and feed-back parts, respectively. Training sequences with an adaptive process using the least-mean-square (LMS) algorithm were applied to train the coefficients of the filter taps. The first 2048 samples of the traces were used as the training sequences. The training process was executed iteratively 10 times with different step sizes varying from 0.03 to 0.003. After the coefficients were trained during the initialization stage, they were kept constant for the whole payload. We used IIR filter instead of decision feedback equalizer (DFE) because the decision of BB8 is not straightforward, where no instant symbol-wise decision can be made. Therefore, we set the decision phase after the equalization and used the IIR filter, where no decision is required in advance. It is noteworthy that for keeping the results comparable, we apply the same signal process on all the formats studied in this work.

Data collections are treated differently in different transmission regimes. 100 traces with 2 million samples (25 μs) were stored for each transmission condition in critical regime: for the received optical power which generates BER approximately lower than 10^{-3} to the maximum received optical power, where the accuracy of BER is easily influenced by the number and length of the traces. 10 traces with 1 million samples (12.5 μs) were stored for the remaining power regime, because the trend was well displayed in the higher noise conditions. The value in every condition was given by the mean value of 90% confidence.

The performance criteria is often defined as the required received optical power with respect to a specific BER threshold. In optical transmission network (OTN) standard, FEC with 7% overhead (OH) is adopted and BER below 3.8×10^{-3} is required as a criterion of successful transmission. However, it is not always reasonable to consider this BER threshold for the short-reach optical interconnects scenario because of high latency and large overhead of OTN FEC. Applications such as intra-datacenter (< 1000 m), rack-to-rack interconnects (from several meters to hundreds meters) and the board-to-board interconnects require the latency less than several hundreds nanoseconds. In addition, the high data exchange rates between datacenters are sensitive to the FEC OH. The newly accepted IEEE 802.3bm standard adopts FEC with a lower BER threshold for 100GBASE-SR4 transmission. The standard includes 2.7% OH Reed-Solomon code, RS (528, 514), with 100 ns latency. These requirements imply BER threshold at 1.42×10^{-5} for output BER lower than 10^{-15} [29], [30]. A non-FEC transmission is preferred for application scenarios with extreme latency requirements, e.g. the data exchange between supercomputers. BER lower than 10^{-12} or even 10^{-15} is required. In our work the 2.7% RS (528, 514) is set as the main criteria, together with the 7% FEC limit at 3.8×10^{-3} and non-FEC limit at 10^{-12} as additional references.

VI. Performance

A. Back-to-back measurements

Fig. 8 shows the BTB BER sensitivity of BB8, PAM-4, and PAM-8. The last one is used as a reference. Substantially, BB8 and PAM-4 perform similarly at the 7% OH FEC level, predicted by simulation shown in Fig. 4. However, in the experiment BB8 has a minor degradation of 0.2 dB to PAM-4. It is reasonable that BB8 degrades faster due to the system imperfection in the low SNR regime, as it is constructed by more neighboring points. With the increase of received optical power, BB8 outperforms PAM-4 by an asymptotic gain larger than 1 dB. An apparent error floor can be observed for the PAM-4's curve due to the limited bandwidth, relative intensity noise (RIN) and laser nonlinearities. Its new counterpart, BB8, provides a potential to achieve BER=10^{-12} before reaching the maximum laser optical output power, as can be concluded from the fitted trend line in Fig. 8. It is also possible that BB8 conceals the error floor below the measurement accuracy limit at BER=10^{-7}. In contrast, PAM-8 displays an unsuccessful transmission with 7% FEC. BB8 gives a 2dB power margin (maximum optical power -2 dBm) at the 2.7% OH FEC of RS (528, 514) which gives the output BER<10^{-15}. PAM-4 has a BER gap larger than one order of magnitude.

B. MMF links

Transmission of BB8 over 100 m OM3 and OM4 MMFs results in a < 1 dB penalty at 7% FEC as compared to the BTB scenario (100 m OM3 in Fig. 9 and 100 m OM4 in Fig. 10). PAM-4 experiences a major degradation in OM3 and OM4. Unlike the simulation analysis in Fig. 4, the receiver sensitivity for BB8 is improved as compared to PAM-4 by 0.6 dB and 1 dB for OM3 and OM4, respectively. BB8 has a successful transmission at the lower FEC threshold and an improved power margin for both 100 m OM3 and 100 m OM4, whereas for PAM-4 the error floor close to maximum received optical power makes 56 Gbit/s transmission unsuccessful. Apparently, PAM-4 degrades faster than BB8 in MMF links. We believe that it stems from the fact that BB8 has larger MMED than PAM-4, which is more tolerant to the signal distortion from the nonlinearities of components and the limited bandwidth of fiber links. It is also noteworthy that the increased gap doesn't imply the inevitable relations with the differences in specifications between OM3 and OM4. In principle, OM4 is further optimized based on OM3, which theoretically should have the larger modal bandwidth. However, due to the different

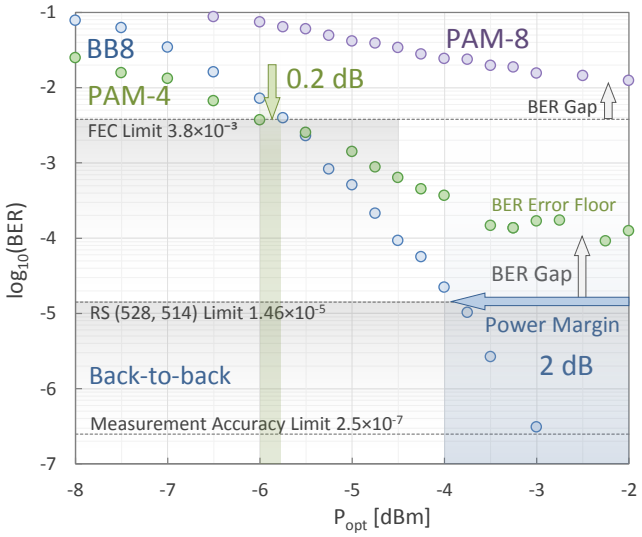

Fig. 8. Comparison of back-to-back BER sensitivity for BB8 (azure), PAM-4 (lemon grass) and PAM-8 (lavender) in 28GBaud/s data-links.

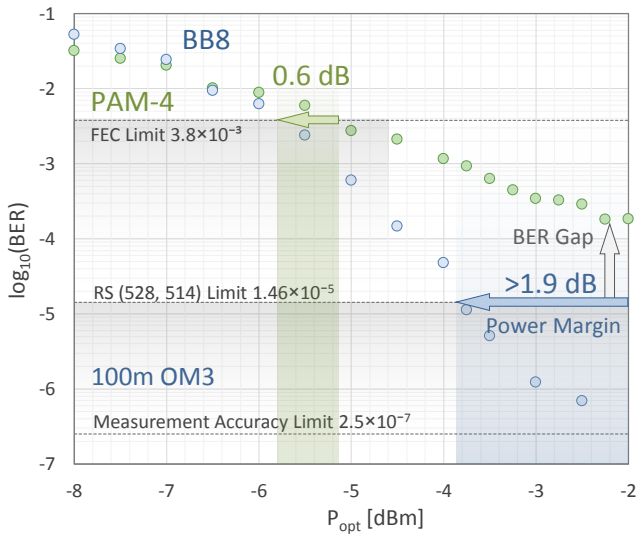

Fig. 9. BER performances of BB8 and PAM-4 with varying received optical power measured for transmission over 100 m OM3 MMF.

design and implementation of vendors, batches, conservation conditions of fiber spools or even launching conditions, it is difficult to provide direct comparison of the performance with different fiber spools. Deeper analysis goes beyond the scope of this paper.

Since 100 m links are typical in commercial products, these results imply the potential of BB8 for MMF data transmission links scenarios.

VII. Conclusion

An 8D modulation format based on E8 lattice was proposed for short-reach data transmission links. The experimental performance shows a 2 dB power margin in BTB measurements and ~ 1.5 dB for a transmission over 100 m OM3/OM4 MMF

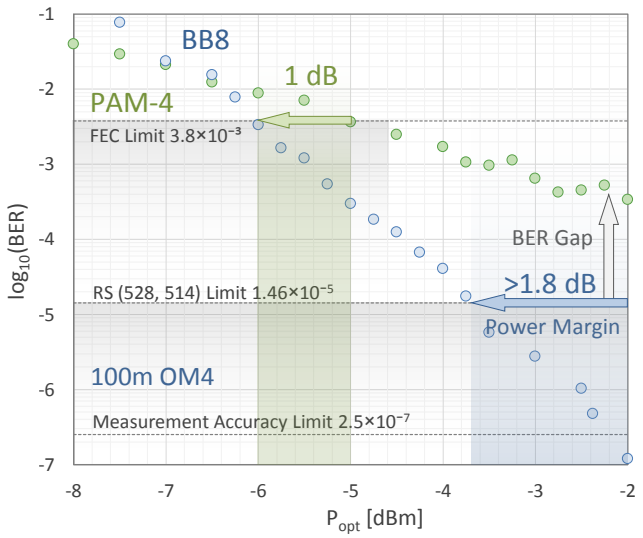

Fig. 10. BER performances of BB8 and PAM-4 with varying received optical power measured for transmission over 100 m OM4 MMF.

measured at 2.7% 100BASE-SR4 FEC. It implies the potential advantages of BB8 in intra-datacenter and other short-reach applications. Due to a better asymptotic BER performance, BB8 relieves the requirement on maximum received optical power, and hence the maximum laser output power. Potential non-FEC transmission of BB8 down to BER=10^{-12} without extra redundancy can provide reduced latency and complexity of the transceivers. Moreover, it is inherently compatible with the 8-lane OSFP links. BB8 is also attractive for future modulation flexible transceivers, because of the possible smooth transition between BB8 and PAM-n provided by the simplified mapping and de-mapping schemes. Considering the requirements on capacity, power efficiency, latency, reliability and flexibility, BB8 is a possible candidate for next generation IM/DD optical interconnections.

Acknowledgment

This work is partly financed by the HOT project of the Danish Innovation Fund, in collaboration with Mellanox Technologies. The authors would like to thank Dr. Henning Bülow from Bell Labs, Nokia for the constructive discussion and Finisar U.S. for the support with VCSELs. We also thank Keysight for providing AWG and DSO.

References

[1] D. M. Kuchta, A. V. Rylyakov, F. E. Doany, C. L. Schow, J. E. Proesel, C. W. Baks, P. Westbergh, J. S. Gustavsson, and A. Larsson, "A 71-Gb/s NRZ modulated 850-nm VCSEL-based optical link," *IEEE Photon. Technol. Lett.*, vol. 27, no. 6, pp. 577–580, Mar. 2015.

[2] K. Szczerba, P. Westbergh, M. Karlsson, P. A. Andrekson, and A. Larsson, "70 Gbps 4-PAM and 56 Gbps 8-PAM using an 850 nm VCSEL," *J. Lightw. Technol.*, vol. 33, no. 7, pp. 1395–1401, Apr. 2015.

[3] J. Castro, R. Pimpinella, B. Kose, Y. Huang, B. Lane, K. Szczerba, P. Westbergh, T. Lengyel, J. Gustavsson, A. Larsson, and P. Andrekson, "Investigation of 60 Gb/s 4-PAM using an 850 nm VCSEL and multimode fiber," *J. Lightw. Technol.*, vol. 34, no. 16, pp. 3825–3836, Aug. 2016.

[4] K. Szczerba, M. Karlsson, P. Andrekson, A. Larsson, and E. Agrell, "35.2 Gbps 8-PAM transmission over 100 m of MMF using an 850 nm VCSEL," in *Proc. ECOC*, London, UK, Sep. 2013, paper Th.1.F.1.
[5] W. A. Ling, I. Lyubomirsky, R. Rodes, H. M. Daghighian, and C. Kocot, "Single-channel 50G and 100G discrete multitone transmission with 25G VCSEL technology," *J. Lightw. Technol.*, vol. 33, no. 4, pp. 761–767, Feb. 2015.
[6] R. Puerta, M. Agustin, L. Chorchos, J. Tonski, J.-R. Kropp, N. Ledentsov, V. A. Shchukin, N. N. Ledentsov, R. Henker, I. T. Monroy, J. J. V. Olmos, and J. Turkiewicz, "107.5 Gb/s 850 nm multi- and single-mode VCSEL transmission over 10 and 100 m of multi-mode fiber," in *Proc. IEEE OFC*, Anaheim, CA, USA, Mar. 2016, paper Th5B.5.
[7] E. Agrell and M. Karlsson, "Power-efficient modulation formats in coherent transmission systems," *J. Lightw. Technol.*, vol. 27, no. 22, pp. 5115–5126, Nov. 2009.
[8] M. Karlsson and E. Agrell, "Which is the most power-efficient modulation format in optical links?" *Opt. Exp.*, vol. 17, no. 13, pp. 10 814–10 819, Jun. 2009.
[9] J. Karout, X. Liu, C. Sethumadhavan, E. Agrell, M. Karlsson, and R. Essiambre, "Experimental demonstration of an optimized 16-ary four-dimensional modulation format using optical OFDM," in *Proc. IEEE OFC/NFOEC*, Anaheim, CA, USA, 2013, paper OW3B.4.
[10] H. Bülow, "Polarization QAM modulation (POL-QAM) for coherent detection schemes," in *Proc. IEEE OFC/NFOEC*, San Diego, CA, USA, Mar. 2009, paper OWG2.
[11] H. Bülow, X. Lu, L. Schmalen, A. Klekamp, and F. Buchali, "Experimental performance of 4D optimized constellation alternatives for PM-8QAM and PM-16QAM," in *Proc. IEEE OFC*, San Francisco, CA, USA, Mar. 2014, paper M2A.6.
[12] J. K. Fischer, S. Alreesh, R. Elschner, F. Frey, M. Nölle, C. Schmidt-Langhorst, and C. Schubert, "Bandwidth-variable transceivers based on four-dimensional modulation formats," *J. Lightw. Technol.*, vol. 32, no. 16, pp. 2886–2895, Aug. 2014.
[13] A. Alvarado and E. Agrell, "Achievable rates for four-dimensional coded modulation with a bit-wise receiver," in *Proc. IEEE OFC*, San Francisco, CA, USA, 2014, paper M2C.1.
[14] T. A. Eriksson, T. Fehenberger, P. A. Andrekson, M. Karlsson, N. Hanik, and E. Agrell, "Impact of 4D channel distribution on the achievable rates in coherent optical communication Experiments," *J. Lightw. Technol.*, vol. 34, no. 9, pp. 2256–2266, May 2016.
[15] J. K. Fischer, C. Schmidt-Langhorst, S. Alreesh, R. Elschner, F. Frey, P. Wilke-Berenguer, L. Molle, M. Nölle, and C. Schubert, "Generation, transmission, and detection of 4-D set-partitioning QAM signals," *J. Lightw. Technol.*, vol. 33, no. 7, pp. 1445–1451, Apr. 2015.
[16] T. Koike-Akino, D. S. Millar, K. Kojima, and K. Parsons, "Eight-dimensional modulation for coherent optical communications," in *Proc. ECOC*, London, UK, Sep. 2013, paper Tu.3.C.3.
[17] M. Nakamura, M. Yoshida, F. Hamaoka, and K. Yonenaga, "Optical 8-dimensional time-polarization modulation using square- QAM-constellation and a simple decoding algorithm," in *Proc. OECC*, Shanghai, China, Jun. 2015, paper JTHA.33.
[18] S. Ishimura and K. Kikuchi, "Multi-dimensional permutation-modulation format for coherent optical communications," *Opt. Exp.*, vol. 23, no. 12, pp. 15 587–15 597, Jun. 2015.
[19] D. S. Millar, T. Koike-Akino, S. O. Arik, K. Kojima, K. Parsons, T. Yoshida, and T. Sugihara, "High-dimensional modulation for coherent optical communications systems," *Opt. Exp.*, vol. 22, no. 7, pp. 8798–8812, Apr. 2014.
[20] J. Karout, E. Agrell, K. Szczerba, and M. Karlsson, "Optimizing constellations for single-subcarrier intensity-modulated optical systems," *IEEE Trans. Inf. Theory*, vol. 58, no. 7, pp. 4645–4659, Jul. 2012.
[21] W. Mao and J. M. Kahn, "Lattice codes for amplified direct-detection optical systems," *IEEE Trans. Commun.*, vol. 56, no. 7, pp. 1137–1145, Jul. 2008.
[22] J. Renaudier, R. Rios-Müller, M. A. Mestre, H. Mardoyan, A. Konczykowska, F. Jorge, B. Duval, and J. Dupuy, "Multi rate IMDD transceivers for optical interconnects using coded modulation," in *Proc. IEEE OFC*, Anaheim, CA, USA, 2016, paper Tu2J.2.
[23] R. Rios-Müller, J. Renaudier, M. A. Mestre, H. Mardoyan, A. Konczykowska, F. Jorge, B. Duval, and J. Dupuy, "Multi-dimension coded PAM4 signaling for 100Gb/s short-reach transceivers," in *Proc. IEEE OFC*, Anaheim, CA, USA, 2016, paper Th1G.4.
[24] N. Stojanovic, C. Prodaniuc, F. Karinou, and Z. Qiang, "56-Gbit/s 4-D PAM-4 TCM transmission evaluation for 400-G data center applications," in *Proc. IEEE OFC*, Anaheim, CA, USA, 2016, paper Th1G.6.
[25] C. Prodaniuc, N. Stojanovic, Z. Qiang, F. Karinou, T. Lee, K. Engenhardt, and R. Llorente, "Experimental demonstration of 56 Gb/s 4D-PAM-5 Trellis coded modulation for 400G WDM metro-access networks," in *Proc. IEEE OFC*, Anaheim, CA, USA, 2016, paper Tu2A.6.
[26] X. Lu and I. T. Monroy, "8-dimensional lattice optimized formats in 25-GBaud/s VCSEL based IM/DD optical interconnections," in *Proc. ACP*, Hong Kong, China, 2015, paper AS4D.3.
[27] X. Lu, A. Tatarczak, and I. T. Monroy, "Eight Dimensional Optimized Modulation for IM-DD 56 Gbit/s Optical Interconnections Using 850 nm VCSELs," in *Proc. ECOC*, Düsseldorf, Germany, 2016, paper Tu.1.C.2.
[28] J. H. Conway, N. J. A. Sloane, and E. Bannai, *Sphere-packings, Lattices, and Groups*. New York, NY, USA: Springer-Verlag New York, Inc., 1987.
[29] "IEEE standard for Ethernet - amendment 3: physical layer specifications and management parameters for 40 Gb/s and 100 Gb/s operation over fiber optic cables," *IEEE Std 802.3bm-2015 (Amendment to IEEE Std 802.3-2012 as amended by IEEE Std 802.3bk-2013 and IEEE Std 802.3bj-2014)*, pp. 1–172, Mar. 2015.
[30] J. Petrilla, "100G SR4 & RS (528, 514, 7, 10) FEC," Avago Technologies, Tech. Rep., Sep. 2012.

Xiaofeng Lu received his M.Sc. degree in photonics from Universität Erlangen-Nürnberg, Germany, in 2014, with projects on ultra-high speed coherent transmission accomplished in Bell Labs, Nokia, Germany . He is currently working toward the Ph.D. degree in the Department of Photonics Engineering, Technical University of Denmark, with HOT project on high-speed optical interconnects, in collaboration with Mellanox Technologies. His research interests include high speed optical inter-and intra-datacenter interconnects, digital signal processing, nonlinearity mitigation in coherent transmission and machine learning used in optical communication.

Anna Tatarczak received her PhD degree at the Department of Photonics Engineering, Technical University of Denmark, in 2016. She received double Bachelor of Science degrees in Systems & Networks, as well as in Management in Telecommunications from Warsaw University of Technology, Poland, in 2010. She earned her Master of Science degree in Telecommunications from the Technical University of Denmark in 2013. Her research interests include optical systems design and short-reach optical communication.

Vladimir Lyubopytov received his Candidate of Science degree in Telecommunication Systems, Networks and Devices from Ufa State Aviation Technical University, Russia, in 2013. He is currently doing his postdoctoral research at the Department of Photonics Engineering, Technical University of Denmark, with HOT project on high-speed optical interconnects, in collaboration with Mellanox Technologies. His research interests include digital and optical signal processing, high-capacity optical fiber communications, and singular optics.

Idelfonso Tafur Monroy is currently a Professor and the Head of the Metro-Access and Short Range Systems group of the Department of Photonics Engineering at the Technical University of Denmark. He graduated from the Bonch-Bruevitch Institute of Communications, St. Petersburg, Russia, in 1992, where he received a M.Sc. degree in multichannel telecommunications. In 1996 he received a Technology Licentiate degree in telecommunications theory from the Royal Institute of Technology, Stockholm, Sweden. In the same year he joined the Electrical Engineering Department of the Eindhoven University of Technology, The Netherlands, where he earned a Ph.D. degree in 1999 and worked as an Assistant Professor until 2006. He is currently involved in the ICT European projects GigaWaM and EURO-FOS and is the technical coordinator of the CHRON project. His research interests are in hybrid optical-wireless communication systems, high-capacity optical fiber communications, digital signal processing for optical transceivers for baseband and radio-over-fiber links, application of nanophotonic technologies in the metropolitan and access segments of optical networks as well as in short range optical-wireless communication links.